nature electronics

Article

https://doi.org/10.1038/s41928-023-01029-4

Spin-acoustic control of silicon vacancies in 4H silicon carbide

In the format provided by the authors and unedited

SUPPLEMENTAL INFORMATION FOR "SPIN-ACOUSTIC CONTROL OF SILICON VACANCIES IN 4H SILICON CARBIDE"

Jonathan R. Dietz[†1], Boyang Jiang[†2], Aaron M. Day [1], Sunil A. Bhave[2] and Evelyn L. Hu[1]

[1] John A. Paulson School of Engineering and Applied Sciences, Harvard University, Cambridge, MA. 02138, USA

[2] OxideMEMS Lab, Purdue University, West Lafayette, IN. 47907, USA

[†] Equally contributing authors

Contents

1. Power Dependence of ODSAR

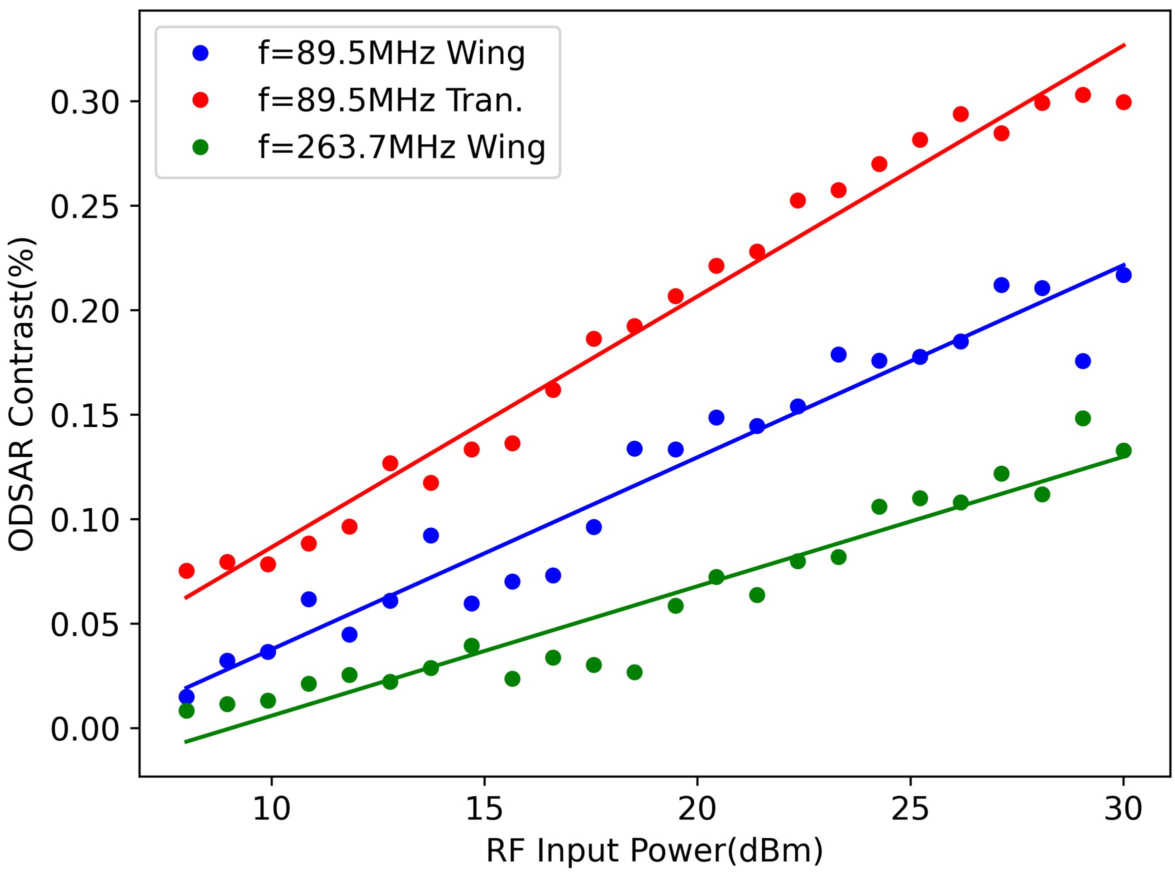

SupplementalFigure 1. Power dependence of ODSAR intensity for low and frequency modes, on and off the transducer region. Even at resonance, the ODSAR signal of the ensemble is characterized by the broadband piezo-transduction described in the main body of this work. The ODSAR signal shows excellent linearity over the drive powers probed in this experiment. Power is measured at the input port of the device.

Determination of spin resonance intensity at different input powers was also compared in Supplemental Figure 1. We find that all three types of strain induced spin transitions (broadband piezo-electric actuation, flexural resonance, and extensional resonance) have linear power intensity dependence. The lower intensity of the extensional mode spin-acoustic resonance at the same power as flexural mode spin-acoustic resonance corroborates the prediction of lower shear strain by half from our electromechanical model. It is also important to note that even at acoustic resonance, broadband piezo transduction dominates spin dynamics near the transducer.

2. LOBAR Electro-Mechanical Characteristics

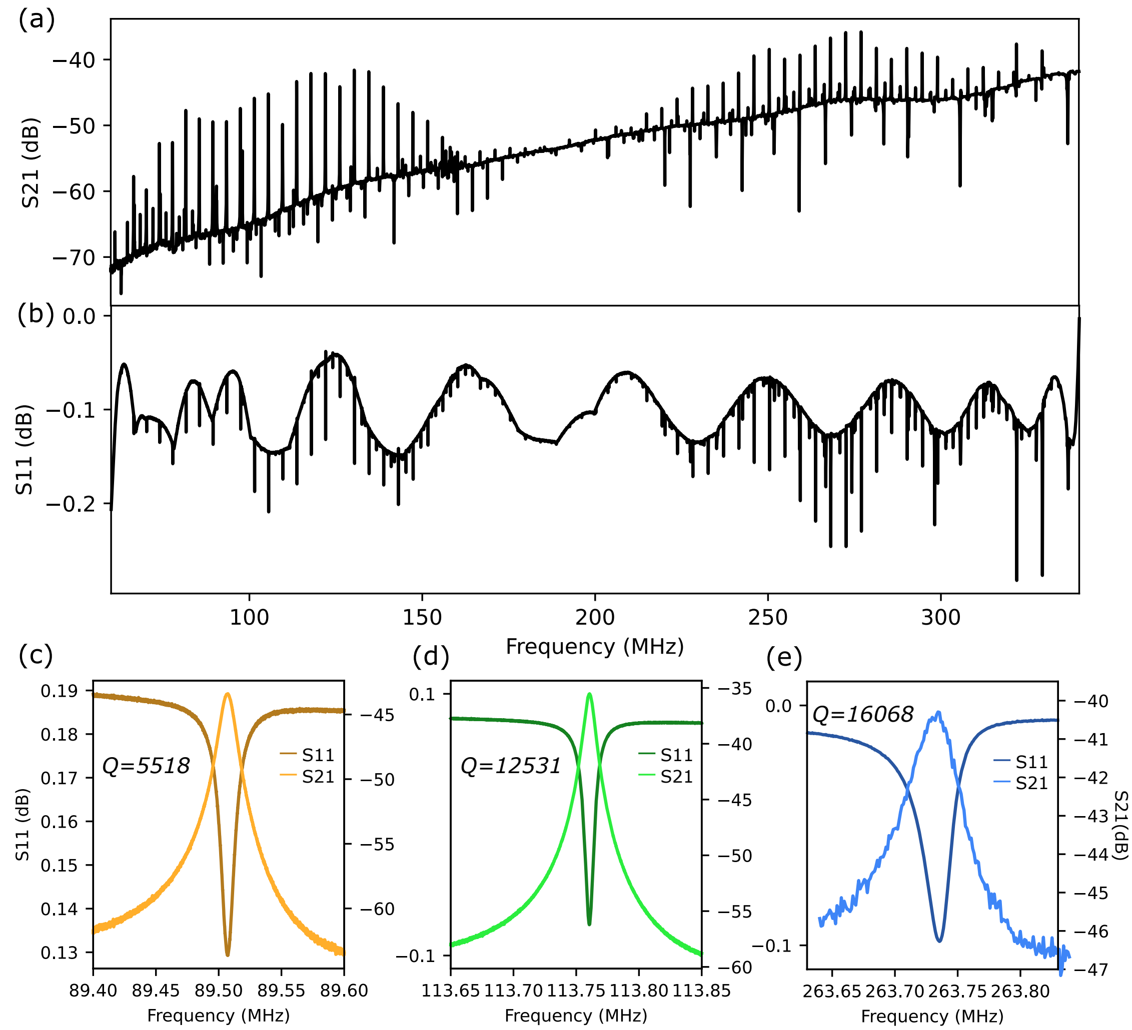

SupplementalFigure 2. Uncalibrated two-port electrical measurements of the device showing (a) S21 and (b) S11 with the S11 and S21 of three modes (c-e) and their qualities factors (Q) calculated from fitting to a Lorentzian distribution. We note that difference between narrowband and broadband measurements are as a result of the uncalibrated nature of the measurement and being taken at different times.

Here we supplement the information provide in the body of the work with additional information about electrical characteristics of the devices. From Supplemental Figure 2a and 2b, we can easily see that the input impedance of the device is not well matched to the driving RF signal, resulting in a lower conversion efficiency of the RF signal into acoustic energy.In the high frequency region (200-300MHz) of the spectrum, there is the continued presence of smaller peaks in between the higher peaks, which have been established to correspond to the device extensional modes via ODSAR. These smaller peaks are most likely high frequency A0 flexural modes of the device, because they have a free spectral range which matches the lower frequency data. We also show a comparison of the electro-mechanical quality factor (Q) of two different A0 flexural modes (Supp. Fig. 2c-d) and one extensional mode (Supp. Fig. 2e).

3. Comparison of ODSAR to Finite Element Strain Model

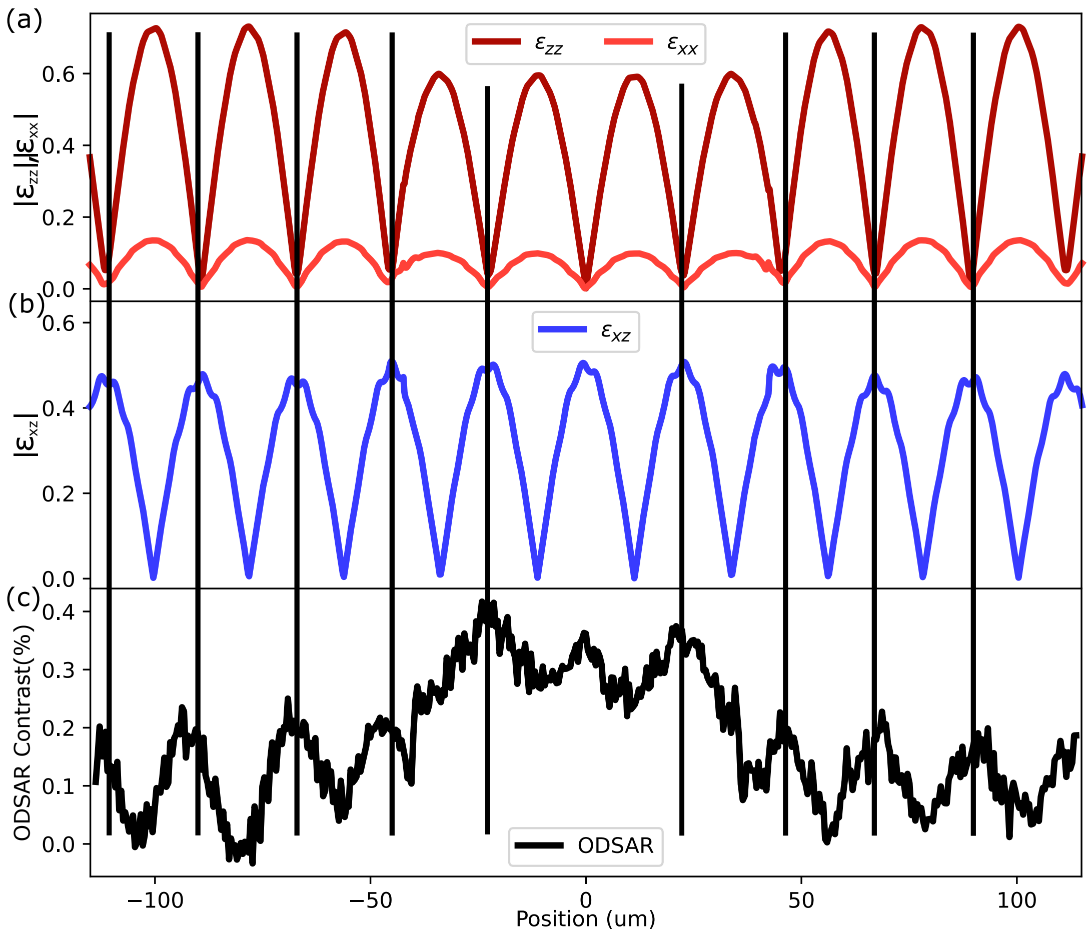

SupplementalFigure 3. Comparison of the (a,b) modeled stress distribution from COMSOL simulation with (c) experimentally measured ODSAR for the low frequency 89.5MHz flexural (A0) mode of the LOBAR scanning along the device x-axis (see Fig.1b.) focused around the center of the device, called the "transducer" in the main section of our work. For comparison, guidelines are drawn between corresponding peaks in the shear stress distribution and ODSAR line scan.

Here we present a more detailed comparison between the results of our finite element COMSOL analysis of the LOBAR and the experimentally measured ODSAR distribution. As shown in Supplemental Figure 3, there is a strong correspondence between the measured intensity of the spin resonance to the theoretically predicted shear strain and not with the bulk strain distribution.

The same is true of the higher frequency extensional modes in the resonator. When comparing the fringe pattern observed in Supplemental Figure 4, the experimentally measured distribution once again best matches the pattern of the shear strain distribution. More significantly the reduced intensity of the shear strain as compared to the flexural mode, shown in Supplemental Figure 3, is also corroborated by our results. This shows that our method is sensitive to the different strain components that are generated by the device.

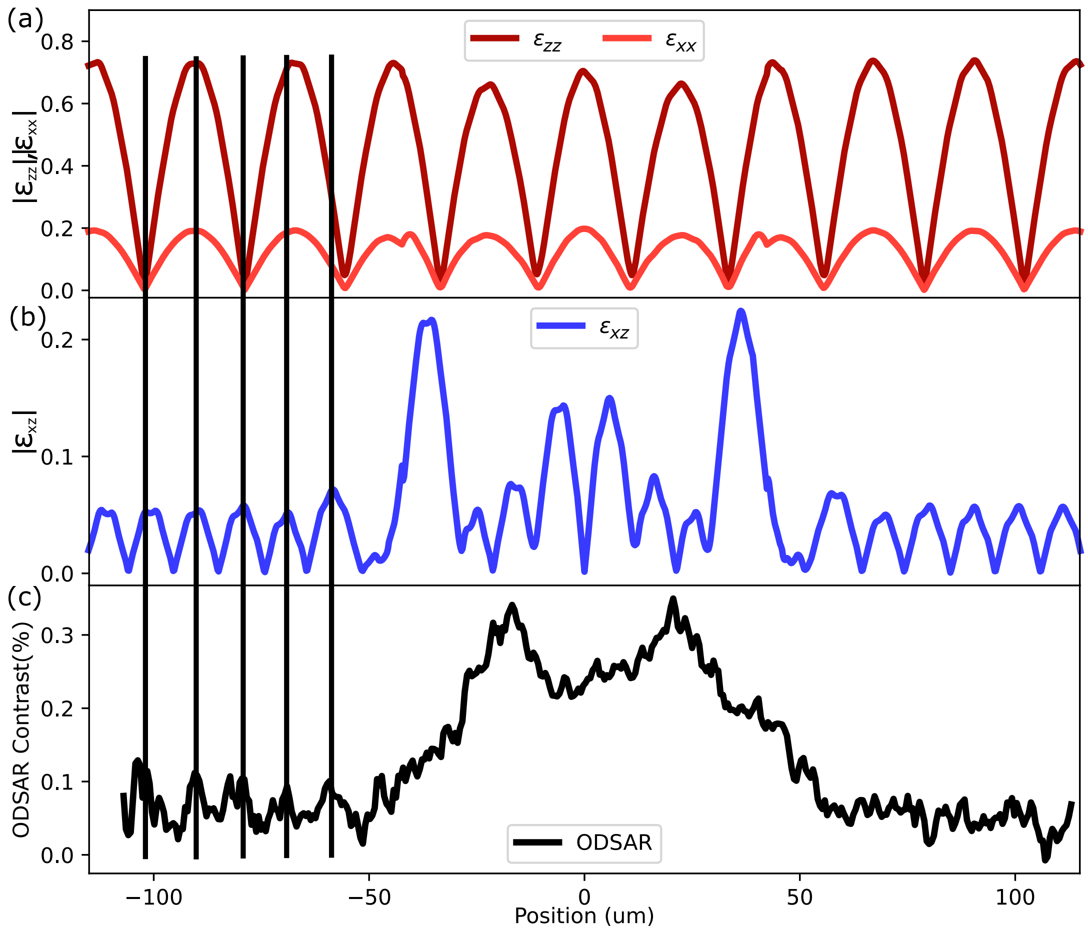

SUPPLEMENTALFIGURE 4. Comparison of the (a,b) modeled stress distribution from COMSOL simulation with (c) experimentally measured ODSAR for the high frequency 263.7MHz extensional (S0) mode of the LOBAR scanning along the device x-axis (see Fig.1b.) focused around the center of the device, called the "transducer" in the main section of our work. For comparison, guidelines are drawn between corresponding peaks in the shear stress distribution and ODSAR line scan.

4. Characterisation of an Etching Asperity

Etching asperities are pits formed during the deep etching of MEMS such as the LOBAR investigated in this study. These imperfections are readily identified by optical and electron microscope and can be studied using profilometry, however the impact of this imperfection on the performance of bulk acoustic resonators is not well understood because of the lack of depth sensitive stress measurements. However, Supplemental Figure 5 demonstrates the acoustic signature of such an etching asperity in the device. In contrast to an expected diminution of stress intensity, the ODSAR shows little perturbation and has a wavelength that matches the predicted acoustic wavelength in the device (Supp. Fig. 5b). This result suggests that shallow asperities (e.g. the 0.8um profiled in Supplemental Figure 5c) have little impact on the microscopic stress distribution underneath them. The minimal impact of the asperity on the strain distribution underneath it supports the notion that bulk acoustics are resistant to the impact of surface imperfections, so long as the acoustic energy is concentrated away from the surface of the material. More photoluminescence signal could improve the signal-to-noise of our ODSAR contrast and give a deeper understanding of the sub-acoustic wavelength impact of surface imperfections like this asperity.

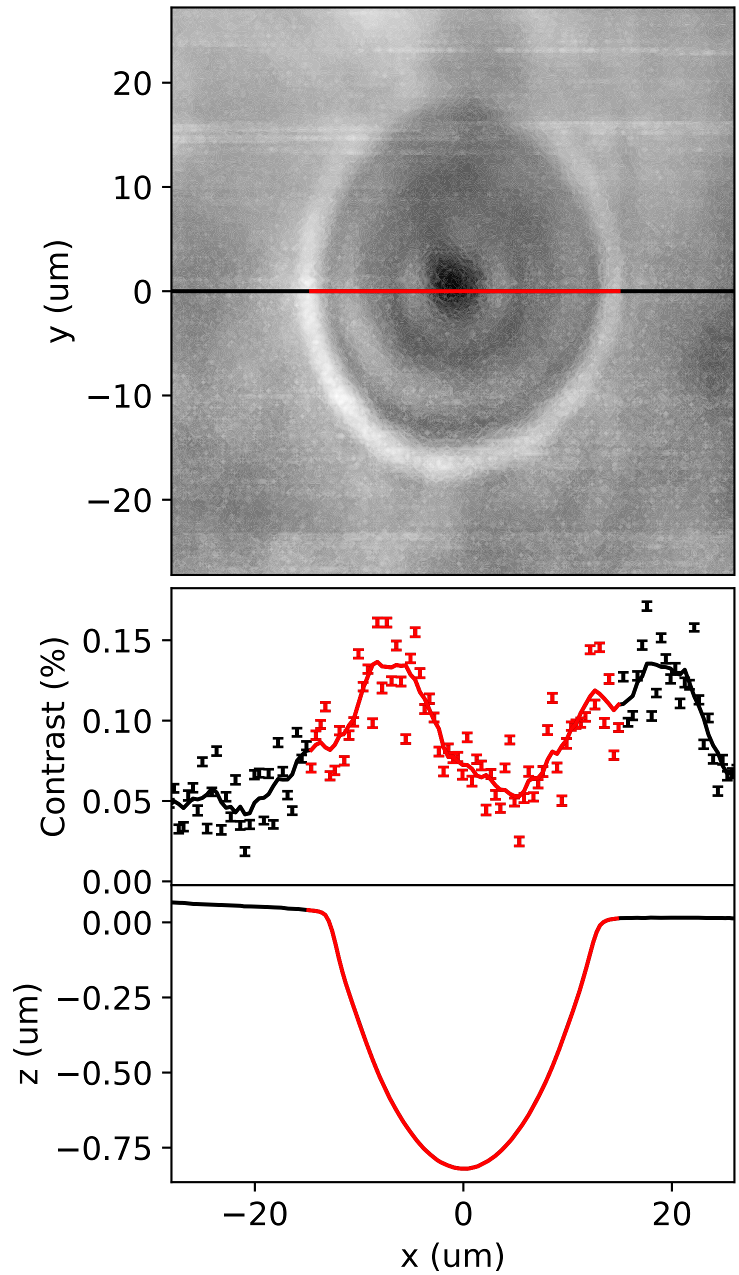

SupplementalFigure 5. Scanning ODSAR measurement of an etching asperity on the device using the technique outlined in the body of the work. (a) Confocal photoluminescence map of the etching asperity. (b) 89.5 MHz resonance scan along the x-direction of the resonator (along the flexural mode fringes) (see Fig.1b), with Fourier transform smooth trend line (c) White light optical profilometry measurement of the etching asperity. In all figures, the red highlighted region outlines the spatial extent of the asperity. Error bars represent the standard deviation of the ODSAR measurement.

5. Optical Measurement Setup

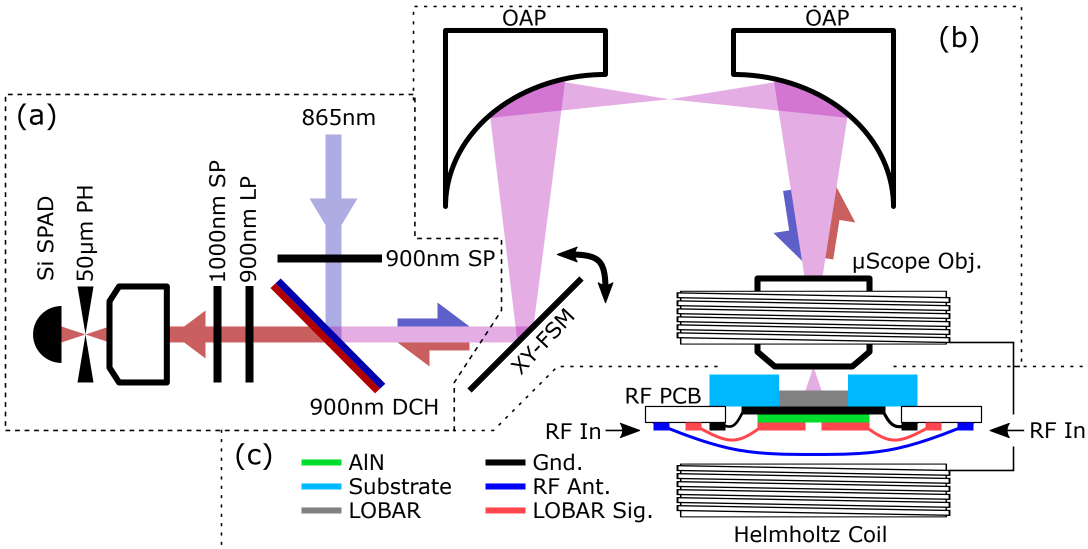

SupplementalFigure 6. Experimental setup used for ODSAR, ODMR, and Rabi oscillation measurements. (a) Silicon vacancies are excited with 5mW of 865nm light filtered by a 900nm short pass (SP) filter. Photoluminescence is collected in reflection and separated from excitation by a 900nm dichroic (DCH), then filtered by a 900-1000nm bandpass before being spatially filtered by a 50um pinhole and then detected by a silicon single-photon avalanche detector (Si SPAD). (b) Confocal scans are carried out with a reflective confocal scanning system consisting of two parent off-axis parabolic mirrors (OAP) sharing the same focal plane, to map the angular deflection of the fast steering mirror (XY-FSM) to a spatial deflection on the sample with a microscope objective (µScope Obj.). (c) The sample is excited from the deeply etched (by reactive ion etching) backside of the LOBAR to allow probing of the wings of the device and the area underneath the transducer (see main work for device area definitions). The RF signal is applied differentially to the device for ODSAR via the interdigital electrodes (LOBAR Sig.). The RF signal is applied via the RF Antenna (RF Ant.) for ODMR measurements. C-axis aligned magnetic field is applied via a pair of Helmholtz coils from 0-200Gauss.